Published in final edited form as:
Cancer Res. 2009 October 1; 69(19): 7557–7568. doi:10.1158/0008-5472.CAN-09-0270.

Molecular distinctions between the stasis and telomere attrition senescence barriers demonstrated by long-term culture of normal human mammary epithelial cells

James C. Garbe[1], **Sanchita Bhattacharya**[1], **Batul Merchant**[1], **Ekaterina Bassett**[1,2], **Karen Swisshelm**[3], **Heidi S. Feiler**[1], **Andrew J. Wyrobek**[1], and **Martha R. Stampfer**[1]

[1] Life Sciences Divisions, Lawrence Berkeley Laboratory, Berkeley, CA

[3] Department of Pathology, University of Colorado Health Sciences Center, Denver, CO

Abstract

Normal human epithelial cells in culture have generally shown a limited proliferative potential of ~10–40 population doublings before encountering a stress-associated senescence barrier (stasis) associated with elevated levels of cyclin-dependent kinase inhibitors p16 and/or p21. We now show that simple changes in media composition can expand the proliferative potential of human mammary epithelial cells (HMEC) initiated as primary cultures to 50–60 population doublings, followed by p16(+), senescence-associated β-galactosidase(+) stasis. We compared the properties of growing and senescent pre-stasis HMEC with growing and senescent post-selection HMEC, i.e., cells grown in a serum-free medium that overcame stasis via silencing of p16 expression and that display senescence associated with telomere dysfunction. Cultured pre-stasis populations contained cells expressing markers associated with luminal and myoepithelial HMEC lineages in vivo, in contrast to the basal-like phenotype of the post-selection HMEC. Gene transcript and protein expression, DNA damage-associated markers, mean TRF length, and genomic stability, differed significantly between HMEC populations at the stasis vs. telomere dysfunction senescence barriers. Senescent isogenic fibroblasts showed greater similarity to HMEC at stasis than at telomere dysfunction, although their gene transcript profile was distinct from HMEC at both senescence barriers. These studies support our model of the senescence barriers encountered by cultured HMEC in which the first barrier, stasis, is Rb-mediated and independent of telomere length, while a second barrier (agonescence or crisis) results from telomere attrition leading to telomere dysfunction. Additionally, the ability to maintain long-term growth of genomically stable multi-lineage pre-stasis HMEC populations can greatly enhance experimentation with normal HMEC.

Keywords

senescence; stasis; human mammary cells; telomere attrition; oxytocin

Introduction

Human epithelial cell culture systems provide experimentally tractable means to examine the processes involved in normal human cell biology, aging and carcinogenesis, but the limited proliferative potential of epithelial cells cultured from normal human tissues has constrained

corresponding author: Martha Stampfer, Lawrence Berkeley National Laboratory, 1 Cyclotron Rd., Berkeley, CA 94720-8174, 510 486-7273, mrstampfer@lbl.gov.
[2]Current Address: Geron Corp., Menlo Park, CA

such studies. While cultured human fibroblastic cells generally display 50–80 population doublings (PD), most published reports on cultured human epithelial cells have shown active growth for only 10–30 PD (1–3), although keratinocytes have proliferated for up to 45 PD (4).

Our previous work culturing human mammary epithelial cells (HMEC) derived from reduction mammoplasty tissues has shown active growth for 10–25 PD, depending upon culture condition, prior to an initial proliferative arrest (1,2,5). Under specific conditions, e.g., exposure to the chemical carcinogen benzo(a)pyrene (6,7), or growth in the serum-free medium MCDB170 (2), rare cells have emerged that lack expression of the cyclin-dependent kinase inhibitor (CKI) $p16^{INK4A}$, and are capable of proliferation for an additional 30–70 PD before encountering a second proliferative arrest (5,8,9). The spontaneous emergence from MCDB170-grown HMEC of rare cells with silenced p16 expression was originally referred to as selection, and the ensuing proliferative population post-selection (2). Due to their increased PD potential, post-selection p16(−) HMEC have been commonly used for examination of supposedly normal finite lifespan HMEC; however, post-selection HMEC can differ significantly from normal HMEC in culture and in vivo (9–14), prompting the need the develop improved methods for normal HMEC culture.

Based on molecular analysis of HMEC phenotypes at these two proliferative barriers, we proposed a new model of the senescence barriers encountered by cultured HMEC (9). In this model, the first barrier, which we have called stasis, is stress-associated and mediated by Rb. The population is arrested in G1, has a low labeling index (LI), and does not show genomic instability or critically short telomeres; virtually all the non-proliferative cells express p16 protein (5). The second barrier is associated with critically shortened telomeres, evidence of DNA damage, and genomic instability, and is a consequence of telomere dysfunction due to ongoing telomere attrition (5,9,15,16). In the presence of functional p53, this barrier has been called agonescence (17); cell populations remain viable, with a LI of ~15%, and arrest at all phases of the cell cycle. If p53 function is abrogated, cells enter crisis and eventually die (9). HMEC at both stasis and agonescence express senescence associated β-galactosidase (SA-β-Gal) activity and display a senescent morphology (9); thus these markers do not distinguish between these distinct senescence barriers.

Based on this model of the senescence barriers, we hypothesized that the limited and variable PD potential of pre-stasis HMEC was due to variable stress exposure under different culture conditions; we therefore looked to determine culture conditions that could increase the PD potential of pre-stasis HMEC. We now report that simple changes in the culture conditions can permit active growth of pre-stasis HMEC for up to 60 PD prior to a p16(+) stasis arrest (low LI, G1 arrest, normal karyotype, variable telomere length). Cells with markers of both myoepithelial and luminal epithelial lineages are present in these populations. This enhanced proliferative potential permits generation of large standardized early passage cell batches that may facilitate experimental examination of normal cultured HMEC, and how these cells transform to malignancy.

Pre-stasis HMEC were further analyzed for gene expression profiling and evidence of DNA damage at increasing passage levels, and these data compared with post-selection HMEC and isogenic human mammary fibroblast cells (HMFC). Our results show significant differences between the pre- and post-stasis HMEC populations. Cells at agonescence had greater evidence of DNA damage than cells at stasis, and distinct gene expression patterns. Gene expression in HMFC at senescence was distinct from HMEC at both stasis and agonescence, although the senescent HMFC resembled HMEC at stasis rather than agonescence in other properties. These data support our model of the mechanistically distinct senescence barriers encountered by cultured HMEC, one associated with stresses, and one associated with telomere dysfunction

due to telomere attrition. Altogether, our findings suggest that the senescence-associated proliferative arrest seen in genomically unperturbed cultured human epithelial and fibroblast cells may be primarily a consequence of exposure to telomere-length independent stresses rather than telomere attrition.

Materials and Methods

Cell Culture

Finite lifespan pre-stasis HMEC from specimens 184 (batch D), 48R (batch T), and 240L (batch B), and post-selection HMEC 184 (batch B, agonescence at ~passage 15), 48R (batch S, agonescence at ~passage 23), and 240L (agonescence at ~passage 18) were obtained from reduction mammoplasty tissue of women aged 21,16, and 19 respectively. Cells were initiated as organoids in primary culture in either serum-free MCDB170 medium (MEGM, Lonza, Walkersville, MD) plus supplements (2), or serum-containing media MM (1) or M85, and subjected to multiple partial trypsinizations, as described (18). Post-selection HMEC were cultured in MCDB170 as described (2,18,19). M85 medium is composed of 50% MM medium and 50% bicarbonate-free supplemented MCDB170; M87 medium is composed of 50% MM4 (MM without the conditioned media)(1) and 50% supplemented MCDB170. Cholera toxin was added to M85 and M87 at a final concentration of 0.5 ng/ml and oxytocin (Bachem) at 0.1 nM. M85A and M87A media were supplemented with 0.1% AlbuMAX I (Invitrogen). Fibroblasts from specimens 184, 48, and 240L were obtained by growing primary reduction mammoplasty cells in DME/F12 with 10% FBS and 10 μg/ml insulin. 250MK cells were obtained from aspirated milk fluids[1].

Total PD level for each culture was calculated beginning at passage 2 using the formula $PD=\log2(N_{final}/N_{initial})$ where $N_{initial}$ is the number of cells seeded in a dish at each passage and N_{final} is the number of cells recovered from the dish. No corrections were made for plating efficiency.

Immunohistochemistry and immunoflourescence

Immunohistochemical analysis for p16 was performed as described using the JC8 antibody (20). SA-β-Gal activity was determined as described (21). Immunoflorescence analysis was performed on cells plated on 4- or 8-well chamber-slides (Lab Tek) as described (9) using 10% goat serum in CAS-block (Zymed) as blocking agent for DNA damage markers and 5% goat serum for cytokeratins and cell surface markers. For DNA damage assays, cells were either irradiated with 10 Gy of ionizing radiation, or mock-irradiated. Antibodies used for immunostaining are listed in Supplementary Table S1. Stained cells were imaged with a Zeiss Axiovert 200M inverted fluorescence microscope and with a Retiga EX camera (Q-Imaging) and Image-Pro®Plus software (MediaCybernetics). Labeling index (LI) was determined using IHC by labeling cells in 35 mm dishes with 10μM BrdU for 24 hr. Labeled cells were fixed with 70% ethanol, rehydrated and treated with 0.1N HCL/0.08% pepsin to denature DNA. Cells were incubated with anti-BrdU antibody (Sigma) overnight at 4°C and bound antibody was detected using the peroxidase mouse ABC kit and DAB substrate kit (Vector Labs).

Mean TRF length and RT-PCR

Mean telomere restriction fragment (TRF) analysis was performed using the TeloTAGGG chemiluminescent telomere length assay (Roche) following the manufacturer's protocol. Genomic DNA was isolated using the Wizard genomic DNA isolation kit (Promega) or by column purification (Qiagen) and 3μg was digested and resolved on 0.8% agarose gels. The

[1]Details on the derivation and culture of these HMEC can be found on our web site: http://hmec.lbl.gov

separated DNA was transferred to a membrane and hybridized overnight to a digoxygenin-labeled telomere specific probe, and washed to remove nonspecific hybrids. Chemiluminescent signal was detected with Kodak Biomax film and quantitated using Imagequant software (Molecular Dynamics). Mean TRF length was calculated as described (22). Quantitative RT-PCR was performed using the Roche Lightcycler and FastStart DNA Master SYBR Green I reagents. First strand cDNA synthesis used the Superscript III synthesis system for RT-PCR (Invitrogen). Transcript levels were normalized to expression of H6PD.

FACS

Cells were fed 48 and 24 hours prior to harvest, collected by trypsinization, rinsed with PBS and fixed with 70% ethanol. Fixed cells were rehydrated in PBS containing 0.1% BSA and 0.05% Tween20, treated with RNAse A (1 μg/mL), and stained with propidium iodide (50 μg/mL). Analyses of total DNA content were performed using a Becton-Dickinson FacScan flow cytometer. The fraction of cells in each cell cycle phase was calculated using the Mod-Fit software program (Verity Software House).

Karyology

HMEC grown in M85±oxytocin were exposed overnight to a 0.01 μg/ml concentration of colcemid (Gibco) when they were around one passage from stasis. Following trypsinization, metaphase cells were collected in hypotonic buffer (0.075M KCl) and incubated at 37°C for 30 min followed by fixation in 3:1 methanol:glacial acetic acid. Trypsin G-banding was performed following standard procedures (23).

RNA Isolation and GeneChip Hybridization

Sub-confluent cultures were harvested for RNA 24 hr following feeding. Cells were lysed with TriZol reagent (Invitrogen) and RNA isolated according to manufacturer's protocol. RNA was further purified by column chromatography (Qiagen) and RNA quality was verified using an Agilent 2100 BioAnalyzer. RNA samples for gene expression analysis were processed and hybridized to Affymetrix HT HG-U133A chips containing ~22,000 probe sets with ~13,000 well annotated genes (Affymetrix) at the LBNL Gene Expression Core facility.

Statistical and Bioinformatics analyses

The raw probe level intensity data captured in .cel files for each chip were processed for background correction, normalization and summarization using Probe-Level Linear Models in LIMMA (Linear Models for Microarray data) module in Bioconductor package[2] (24). Quality measures such as the 3′/5′ ratios of house keeping genes, RNA degradation indices and NUSE (Normalized Unscaled Standard Error) values[3] were used to assess the data, leading to four outlier chips in the dataset being excluded from downstream analysis. Probe sets with intensities 2σ below average background across the chips were filtered out, leaving a total of 9,702 genes (13,791 probe sets). Differentially expressed genes were identified by the empirical Bayes linear model fit in LIMMA (25). P-value adjustment for multiple testing was performed to control the False Discovery Rate (26). Genes were considered differentially expressed with the following criteria: (1) ≥ 2 fold differential (positive/negative) expression between the means of two comparison groups, and (2) False Discovery Rate < 10%. Volcano plots were generated using Spotfire version 199.1008[4].

[2]http://www.bioconductor.org/packages/bioc/1.6/src/contrib/html/affyPLM.html
[3]http://www.bioconductor.org/docs/vignettes.html
[4]http://spotfire.tibco.com

Cluster analyses were performed using the Cluster 3.0 program and visualized using Java TreeView. Normalized Log2 gene expression values for stasis and agonescent HMEC were centered by subtracting the mean value of each probe set across the indicated HMEC samples from each measured value. Unsupervised clustering was performed using the 603 genes where one or more samples had a Log2 expression difference of at least ±1.5. Supervised clustering was performed on the 77 genes with the highest variance across all HMEC samples; these were clustered gene-wise with correlation coefficient as a distance measure using the average linkage method (27). Principal Component Analysis (PCA) (28) was performed using Partek® Genomics Suite (version 6.3 Copyright ©2008, Partek Inc., St. Louis, MO, USA). GO Functional classification of differentially expressed genes from each groups were performed using DAVID (29).

Results

Increased proliferative potential of pre-stasis HMEC

Candidate media formulations were tested using frozen stocks of second passage (p) reduction mammoplasty-derived 184 HMEC that had been grown as primary cultures using MM medium. Primary cultures were initiated using intact organoids, which we have shown provide greater PD potential than dissociated single cells (18,30). These preliminary studies indicated that a medium formulation, M85, (consisting of a 1:1 ratio of MM plus cholera toxin (1) and serum-free MCDB 170 plus supplements (2)), increased PD potential, which was further increased by the addition of 0.1nM of the anti-stress peptide oxytocin (X). We next initiated primary organoid cultures from three different individuals (reduction mammoplasty specimens 48R, 184, and 240L) in M85 with and without oxytocin (Fig. 1A). Following our early protocols (18,30), primary cultures were subjected to repeated partial trypsinizations (PTs) to yield multiple second passage cultures that were either stored frozen, or maintained in culture. In this protocol, an epithelial monolayer is allowed to grow out from the organoids until subconfluence, ~50–70% of the cells are removed by trypsinization, and the culture allowed to regrow to subconfluence and subjected to additional PTs. This protocol precludes precise determination of the number of PD in the primary cultures, a value likely to have been at minimum 5–10 PD and possibly 25–30 PD after multiple PTs.

Growth in M85+X was rapid for 25–35 PD, followed by a gradual slow-down with senescence arrest ~45 PD from 2p. In the absence of oxytocin, there was similar initial rapid growth for 20–25 PD, followed by reduced, often heterogeneous proliferation. Growth from 2p of 184 HMEC in MM is shown for comparison. We then formulated a medium that could provide long-term growth without the epithelial cell conditioned media (CM) present in MM. Figure 1B show growth from 2p of 184 HMEC in media containing oxytocin with (M85) or without (M87) CM, in the presence or absence of lipid rich BSA (A). In the presence of oxytocin, the BSA was able to substitute for the CM (M87A+X curve), and provided more PD than the M85 +X medium. We found no significant differences in long-term growth from 2p of 184 HMEC in M85+X and M87+X media under conditions of 20% vs. 3% oxygen (data not shown). Our new media formulations now make possible the generation and frozen storage of large batches of early passage pre-stasis HMEC that retain extensive proliferative potential, thereby permitting reproducible experimentation using standardized HMEC batches from individual specimen donors.

The M85+X medium was used to grow milk-derived HMEC previously grown in MM in primary culture and then stored frozen at 2p (250MK curve in Fig. 1B). These cells also showed an extended PD potential compared to their prior growth in MM (arrest at 10p vs. 3p in MM), with a growth curve similar to that seen in our original testing of 184 HMEC started in MM and switched to M85+X at 2p (not shown). The comparison of the 250MK growth curve with

that of 184D HMEC in M85+X in Fig 1B suggests that total PD potential is significantly reduced when primary cultures are not initiated in the newer media formulations.

The pre-stasis cultures of 184D and 48RT HMEC shown in Fig. 1A were examined at different passage levels for markers of growth (LI) and senescence (expression of p16 and SA-β-Gal). As shown in Fig. 1C for 184D HMEC, with increasing passage in M85+X, the LI decreased, while the number of cells expressing p16 and SA-β-Gal increased. A few, larger cells expressed senescence markers as early as 2p. As cultures neared stasis at 14p, most cells displayed a senescent morphology (large, flat, vacuolated) and expressed p16 and SA-β-Gal, although pockets of proliferative cells (small refractile morphology and positive LI) were still present. 184D HMEC grown without oxytocin also showed a senescent morphology, and expression of p16 and SA-β-Gal, as they approached stasis at 9p. Similar results were seen for 48RT HMEC (not shown).

We previously reported that at a first proliferative barrier, 184 and 48R HMEC and isogenic HMFC were arrested in the G1 phase of the cell cycle (2N to 4N ratio >4) and had normal karyotypes; however, those HMEC cultures had only undergone ~10 PD from passage 2 (5). FACS examination of near stasis populations of 184D and 48RT HMEC grown in M85±X also showed a 2N to 4N ratio of >4 (Table 1). Chromosome studies were performed on 184D and 48RT HMEC near stasis, yielding thirty-five analyzable metaphases (Supplementary Table S2). Thirty-four displayed a normal, 46, XX karyotype. One cell showed a recombinant chromosome derived from chromosomes 1 and 3; such single cell, non-clonal events are frequently observed in cultured normal human cells. These data indicate that although the PD level at which stasis occurs depends upon culture conditions, the phenotype of HMEC at stasis (senescent morphology, SA-β-Gal staining, low LI, expression of p16, arrest in G1 and normal karyotypes) remains similar, and consistent with an Rb-mediated arrest that is independent of telomere length.

Stasis is independent of mean TRF length

Our previous studies reported that post-selection HMEC did not have detectable telomerase activity, and showed ongoing telomere erosion, with evidence of telomere dysfunction when the mean TRF declined to ~4–5 kb (5,9). In contrast, low telomerase activity was seen in some pre-stasis HMEC (15,31), and mean TRF values at stasis were not critically short (~8 kb and ~6 kb when grown in MM or MCDB170 respectively (5,31)). However, the 184 and 48R HMEC examined in those studies grew for only ~15–30 total PD. We now determined whether the extended proliferative potential of pre-stasis HMEC in M85±X led to critically short mean TRF lengths at stasis.

184D HMEC examined at increasing passages (Fig. 2) showed very gradual TRF attrition between passages 2–11. Mean TRF length in 184D grown with oxytocin declined from ~10–11 kb at 2p to ~9 kb at 11p, followed by a steeper decline toward stasis, with a mean TRF length of ~7 kb at 14p (~45–55 total PD). Without oxytocin, the 184D cultures reached stasis at passage 10, and had a mean TRF of ~9.5 kb at 9p (~30–40 total PD), similar to the value seen at the same PD level in the cultures with oxytocin. These results indicate that the mean TRF value at stasis varies depending upon the culture conditions, and is not critically short even after more than 40 PD, consistent with the observed normal karyotype at stasis.

Transcript and protein expression in pre-stasis HMEC

Pre-stasis HMEC populations were characterized for gene transcript profiles and protein expression, with emphasis on examining markers of mammary cell lineage and the effects of passage, senescence, and interindividual differences. 184D and 48RT HMEC were examined for lineage markers by immunofluorescence (IF) at 5p and 13p, and 250MK at 3p; additional

cultures were examined at various passages by immunohistochemistry (IHC) for keratin (K) 19. The 184D, 48RT, and 240LB HMEC grown in M85±X shown in Fig. 1A were examined for gene transcript profiles with increasing passage levels; growing 250MK HMEC were also analyzed (Fig. 3A). Additionally, growing (184B, 48RS, 240L) and agonescent (184B, 48RS) post-selection HMEC, and growing and senescent 184 and 48 HMFC were examined to permit comparisons with the pre-stasis cells (see below). A more extensive analysis of the gene transcript data will be the subject of a separate publication.

Figures 3B–D show cellular morphology and the expression of lineage-specific proteins by light microscopy, IHC, and IF. Fig. 3B illustrates the heterogeneous morphology of 184D passage 3 cultures derived from different PTs. Cells from PT2 contain mostly cobblestone epithelial cells and flatter cells in closed colonies similar to what has previously been described as a luminal morphology (32); cultures from PT16 additionally display a cell type with thin cytoplasmic extensions across other HMEC. As expected, HMEC in the closed colonies stained positive for the luminal marker K19, as did some cells with a more cobblestone appearance (cultures shown from PT15). Figure 3C illustrates protein expression in 48RT passage 5 cultures of genes associated with specific lineages in vivo: muc1 and EpCam are expressed by luminal lineages; K14 by myoepithelial lineages, and K19 by both luminal and stem lineages (33). K19(+), EpCam(+), and muc1(+) cells were seen either interspersed among cells with myoepithelial markers or as small homogenous colonies. Fig. 3D illustrates the expression of luminal markers by almost all the milk-derived 250MK cells at passage 3, indicating that our new media formulations are capable of propagating homogenous luminal HMEC populations.

Figure 3A shows a hierarchical cluster of the gene levels of 77 genes chosen from the top 200 genes with greatest variance across all epithelial samples, plus several hand-picked lineage or differentiation-associated genes (EGFR, KRT14, KRT18, KRT7, PGRMC2, RARA, RARB). Pre-stasis HMEC specimens from the Fig. 1A curves ±X are arranged by increasing passage level. The 250MK samples represent cells with a luminal phenotype, while the post-selection HMEC are known to express mostly myoepithelial lineage markers (32).

The data in Figure 3 illustrate several points about the pre-stasis HMEC. First, genes and proteins of both myoepithelial and luminal epithelial cell lineages are expressed in the pre-stasis populations derived from reduction mammoplasties; however, unlike the milk-derived 250MK, cells with luminal markers made up only 10–25% of the populations. The IF and IHC results (Fig 3B–D) are corroborated by the gene transcript data (Fig. 3A) showing expression of K19, EpCam (TACSTD1), and muc1 in all pre-stasis specimens. Thus our new media can support long-term growth of reduction mammoplasty-derived cells with multiple lineage markers. Second, expression levels of many genes change as the cultures progress from early passages to stasis, with most of the changes seen as the populations approach stasis. This result is not surprising, given the differences in proliferation rate as well as known differences in gene expression at senescence in many cell types. However, it also points out the importance of population doubling level as a significant variable to be identified when examining or comparing normal pre-stasis HMEC. Third, although the transcript profiles from the three individual reduction mammoplasty donors are largely similar, some interindividual differences are present (see also Supplementary Figures S1–2), highlighting the importance of examining multiple individuals. Finally, we observed that the morphology of the cells growing out from the primary organoid cultures changed with ongoing PTs (Fig. 3B). Current studies are utilizing pre-stasis HMEC sorted by lineage markers to identify lineage-specific gene expression.

Altogether, these studies show that pre-stasis HMEC grown in our new formulations provide well-characterized normal populations that maintain long-term active growth of multiple mammary cell types similar to what is seen in vivo. All these HMEC ceased proliferation with a phenotype characteristic of stasis; no spontaneous escape from stasis of any cell growing in

any of these serum-containing media has been observed. These long-term pre-stasis cultures were then used, as described below, to compare growing and senescent populations of pre-stasis and post-selection HMEC, and isogenic HMFC, in order to further define the molecular properties of pre-stasis vs. post-selection HMEC, and the stasis vs. telomere dysfunction proliferation barriers.

DNA damage markers in growing and senescent pre-stasis and post-selection HMEC, and isogenic HMFC

Cultured human fibroblasts nearing senescence have been reported to show increased expression of 53BP1 and γH2AX foci and serine-15 phosphorylated p53, markers usually attributed to DNA damage (34,35). Our previous data and model of the senescence barriers (9) predicted that significant DNA damage would be present at agonescence, but we could not predict the situation for HMEC at stasis. We now used IF to examine and compare the level of 53BP1 and γH2AX foci, and serine-15 phosphorylated p53, in growing and senescent pre-stasis and post-selection HMEC, and isogenic HMFC, to determine if HMEC stasis was associated with markers of DNA damage.

HMEC and HMFC were examined while actively growing, or within one passage from proliferative arrest. 53BP1 foci data is shown in Fig. 4A and Supplementary Table S3, and representative IF images for 53BP1 and γH2AX foci are shown in Fig. 4B. Representative images for serine-15 phosphorylated p53 are shown in Fig. 4CD. Exposure to ionizing radiation (IR) was a positive control. Most of the HMEC populations at stasis and agonescence, as well as the senescent fibroblasts, have ≥1 53BP1 focus per cell. However, the HMEC at stasis, and the senescent fibroblasts, have significantly fewer cells with ≥ 3 foci compared to the HMEC at agonescence, which were more similar to the irradiated cultures in number of foci and expression of activated p53. More foci were detectable in the growing post-selection vs. pre-stasis HMEC and there was a higher number of foci in all 184-derived populations compared to 48R. Notably, the number of foci in the pre-stasis cultures increased with passage, rather than correlating with stasis per se, as the cultures maintained without oxytocin reached stasis 4–5 passages (~15–20 PD) earlier, with fewer foci than the cultures grown for more PD with oxytocin. Similar to the data for 53BP1 and γH2AX foci, activated p53 was evident in both 184B and 48RS HMEC at agonescence, and was lower (184D) or barely detectable (48RT) at stasis. Surprisingly, we did not detect activated p53 in either 184 or 48 HMFC at senescence.

These data are consistent with the model that agonescence is a consequence of DNA damage signals resulting from telomere attrition, whereas the longer mean TRF and absence of genomic instability in the cultures at stasis argue that the lower level of foci seen at stasis are not the result of telomere dysfunction due to telomere attrition. Ongoing proliferation may create conditions that elicit low levels of DNA damage, independent of telomere attrition (34). Diversity among donors in vulnerability to DNA damaging stresses might also influence the level of DNA damage foci observed, possibly accounting for the observed differences between cells from specimens 184 and 48R. Altogether, these results indicate that HMEC stasis is not directly correlated with levels of DNA damage.

Comparison of gene expression in growing and senescent pre-stasis and post-selection HMEC, and isogenic HMFC

To further define the molecular differences and similarities between HMEC arrested at stasis vs. agonescence, the transcriptional profiles of growing and senescent populations of pre-stasis and post-selection HMEC were compared. Additionally, isogenic senescent HMFC were compared to the HMEC at stasis and agonescence.

PCA was applied to visualize correlations in the HMEC and HMFC transcriptional profiles. Figure 5A illustrates that HMEC populations can be distinguished using the first three principal components, which account for 37% of total variation. Several observations can be made: (1) Growing populations were separated from senescent populations along the first principal component. Pre-stasis cultures with mixed growing and senescent cells showed intermediate positions. (2) Pre-stasis cultures were separated from post-selection cultures along the second principal component; cells at stasis are separated from cells at agonescence, and growing pre-stasis and post-selection cells are separated. The distinctions in the transcriptional profiles of HMEC at stasis and agonescence, as well as the similarities, are further illustrated by hierarchical cluster analysis (Supplementary Figure S1), which also shows some interindividual differences. Figure 5B shows the PCA analysis comparing senescent HMFC with HMEC at stasis and at agonescence; three principal components accounted for 54% of the total variation. Senescent HMFC are strikingly separated from both types of senescent HMEC along the first principal component, while the HMEC populations at stasis and agonescence were distinguished along the second principal component. These results indicate a strong cell-type specific contribution to senescent gene expression profiles. Figure 5C compares genes modulated in senescent pre-stasis and post-selection HMEC and HMFC, in relation to their growing populations. A large number of genes were unique to either stasis (451), or agonescence (577), although many genes were modulated at both stasis and agonescence (370). Very few genes that were modulated in senescent HMFC were also modulated in HMEC at stasis or agonescence, and only two genes were in common in all the senescent populations. Figure 5D represents the fold-changes and statistical significance of genes differentially modulated in expression between stasis and agonescence. Functional analyses showed that genes associated with “response to stress” were up-regulated at both barriers, but there was no overlap among the gene in the lists (data not shown).

Ten genes with varying expression among the growing and senescent HMEC populations were chosen for QRT-PCR verification of expression levels (Supplementary Figure S2) using the primers shown in Supplementary Table S4; all results were consistent with the microarray data, although levels of expression varied between HMEC derived from specimens184 and 48R.

Altogether, these data indicate that the HMEC senescence barriers of stasis and agonescence are associated with distinct transcriptional profiles, with some similarities in their gene expression. In contrast, the transcriptional profile of genes modulated in senescent HMFC showed very little overlap with the profiles seen in either type of senescent HMEC.

Discussion

Malignant transformation of normal human epithelial cells requires overcoming tumor suppressor barriers that induce cellular senescence in response to stresses, DNA damage, and telomere attrition. Understanding the molecular bases of these senescence barriers, and how cells bypass or overcome them, can provide valuable information relevant to the etiology of and therapeutic intervention in malignant progression. Based on our long-term studies, we have previously proposed a molecularly defined model of the senescence barriers encountered by cultured HMEC ((9) and Supplementary Fig. S3) that is consistent with observed carcinogenic progression in vivo. Three distinct types of senescence barriers have been observed (5,9,36): stasis, a stress-associated barrier mediated by Rb that arrests cells in G1 with a low LI and normal karyotypes; telomere dysfunction due to telomere attrition that produces genomic instability; oncogene-induced senescence that involves a DNA damage response. Molecular definition of human cell senescence barriers has been hampered by variability among species and cell types in vulnerability and responses to senescence-inducing conditions. Additionally, the limited growth potential of cultured normal human epithelial cells prior to the onset of stasis has constrained experimental examination of these cells. In this report, we describe simple

culture methods that support long-term active growth of normal pre-stasis HMEC that express markers of multiple mammary cell lineages, and the use of these cultures to delineate molecular distinctions between the stasis and telomere dysfunction senescence barriers. These data lend further support to our proposal that the senescence barrier encountered by genomically unperturbed human epithelial and fibroblast cells in culture may be primarily a consequence of exposure to telomere-length independent stresses rather than telomere attrition (9).

Our model of the senescence barriers encountered by cultured HMEC proposed that the observed variable PD potential of HMEC prior to a first proliferative arrest is due to variable stress exposure under different culture conditions (9). Here we demonstrate that simple changes in media composition greatly extend the PD potential of HMEC prior to a p16(+) stasis arrest. We utilized media formulations that combined components of our previous HMEC media, serum-free MCDB170 (2), with serum- and CM-containing MM (i.e., M85) or with MM4 which lacks the CM (i.e., M87)(1,30), plus the anti-stress peptide oxytocin and/or lipid-rich BSA to achieve ~60 PD from reduction mammoplasty-derived HMEC prior to stasis. Proliferation was rapid (~50 PD in 65 days from passage 2) and did not require any special treatment of tissue culture substrates, in contrast to a recent report using the treated Primaria dishes and WIT medium, that achieved ~42 PD total over ~130 days from passage 1 (37). The addition of oxytocin alone gave ~20 PD of increased proliferation, although it had little if any effect on the rapid initial growth rate, suggesting that it acts mainly to delay stasis rather than stimulate proliferation. While oxytocin's role in reducing stress responses at the whole body level is well-known (38), its use to prolong normal human cell growth in culture has not to our knowledge been previously reported. Oxytocin signals via G-coupled receptors, which are found on breast cancer cells, and uses the PI3K and MAPK signal transduction pathways (39–42). Oxytocin has been shown to inhibit proliferation of some human tumor-derived cell lines, including breast, associated with increasing cAMP levels, while stimulating other tumor lines (40) and primary explant cultures of rodent mammary myoepithelial cells (43). Further studies will be needed to elucidate how oxytocin delays the onset of stasis in normal HMEC.

Our new media formulations that support long-term growth of pre-stasis HMEC should facilitate experimental examination of normal HMEC biology. This is particularly important as many studies of "normal" HMEC currently utilize the p16(−) post-selection HMEC, which have been shown in this report and others to display properties distinct from normal pre-stasis HMEC in culture and in vivo (9–14). Notably, as demonstrated by IF, IHC, and gene transcript profiles, our culture conditions supported long-term growth of HMEC with both luminal and myoepithelial lineage markers. Luminal epithelial markers were seen on ~10–25% of reduction mammoplasty-derived cells, with decreased expression of the luminal markers K19 and EpCam with increasing passage. This heterogeneity contrasts with the post-selection HMEC populations, which display predominantly myoepithelial markers at all passages, as well as some limited luminal epithelial marker expression (e.g., sialomucins), but no K19 (7,32). Growing milk-derived HMEC displayed a luminal phenotype. Quantitative analysis of the different lineages present in pre-stasis HMEC by FACS sorting using lineage markers is currently in progress. Interindividual differences were noted in gene expression patterns, particularly at stasis, as well as in levels of DNA damage markers. Together with some of our previous studies demonstrating interindividual differences (44), these results point to the importance of examining HMEC from more than one individual when assessing normal HMEC properties. Our findings also illustrate how markers related to growth and stasis, such as p16, SA-β-gal, LI, and gene expression, varied continuously with passage level, such that information about PD level examined relative to total PD potential of that population can be of crucial significance for interpretation of results, or comparison among cell populations.

Pre-stasis populations also differed from post-selection HMEC in parameters related to telomere dynamics, genomic stability, and DNA damage. Previous studies showed that

agonescence correlates with critically short telomeres (mean TRF ≤ 5 Kb), a p53-dependent DNA damage response, and widespread genomic instability (5,9). Virtually all cell metaphases at agonescence showed gross chromosomal abnormalities and telomere associations. This result indicates that the p53-mediated growth arrest at HMEC agonescence does not occur as soon as a single uncapped telomere appears. Rather, HMEC senescence resulting from telomere attrition is associated with critically short telomeres and genomic instability. In contrast, pre-stasis cultures even after >50 PD reached stasis with a normal diploid chromosome complement, thus avoiding the acquisition of many uncharacterized genomic errors as occurs in post-selection HMEC approaching agonescence. Determination of mean TRF lengths indicated, as expected from previous studies, that stasis occurred independent of telomere length. In the situations we have observed thus far, stasis occurred prior to the appearance of critically short telomeres, with a mean TRF of ~6–9 Kb. However, it is theoretically possible that normal pre-stasis HMEC could proliferate to the point of reaching critically short telomeres and agonescence prior to encountering stasis, if grown under very low stress culture conditions. Consistent with the non-critically short TRF length and genomic stability of HMEC at stasis, cells at stasis exhibited greatly reduced levels of markers of DNA damage (53BP1 and γH2AX foci, serine-15 phosphorylated p53) compared to cells at agonescence. Levels of DNA damage markers increased with increasing PD level, and did not correlate with stasis per se, arguing against HMEC stasis being a consequence solely of DNA damage signals.

Altogether, the comparisons shown here and previously of growing and senescent pre-stasis and post-selection HMEC support our model (Sup. Fig. S3) of two molecularly distinct senescence barriers: stasis, resulting from chronic or acute stresses, and telomere dysfunction (agonescence or crisis) due to telomere attrition. Our model is consistent with observations from in vivo carcinoma progression; early stage lesions frequently exhibit errors in the Rb pathway (e.g., loss of p16 expression), while DCIS is associated with short telomeres and genomic instability (16). In vivo, HMEC may also be subject to OIS, and errors that allow this barrier to be overcome could influence the cells' ability to overcome stasis and/or telomere dysfunction.

Transcriptional profiles indicated substantial differences between HMEC stasis and agonescence, as well as between both types of HMEC senescence and HMFC senescence. Bioinformatics analyses showed that the majority of genes modulated at stasis and agonescence were distinct, although there was also significant overlap. The transition from growing post-selection to agonescence was associated with inflammation and telomere processes, which have been implicated in cancer progression. Bioinformatics analyses also demonstrated that HMFC utilize different biological processes than HMEC when transitioning from growing to senescence. As HMFC senesced, they upregulated genes associated with cell communication and downregulated genes associated with cell differentiation. The differential utilization of genes between the two transitions in HMEC and the transition in HMFC is remarkable, with only 2 genes whose modulation is in common between all three transitions. This lack of overlap between genes modulated in HMEC and HMFC senescence is consistent with previous reports comparing post-selection HMEC and mammary fibroblasts, which also showed that genes associated with stress response, cell signaling, cell proliferation, and cell adhesion are significantly enriched in HMEC at what we have called agonescence (45). The striking difference in gene expression between the senescent HMFC and HMEC clearly illustrates cell type specificity in biological processes associated with senescence.

Although the gene transcripts of senescent HMFC were distinct from senescent HMEC, in other properties examined the senescent HMFC resembled HMEC at stasis, and differed from HMEC at agonescence. Like HMEC at stasis, senescent HMFC show a low LI, arrest in G1, expression of p16, absence of critically short telomeres or genomic instability (5), and low or absent DNA damage markers. Given the greater resemblance of senescent HMFC to HMEC

at stasis vs agonescence, it is most likely that they too are arresting at a stasis-like senescence barrier rather than as a consequence of telomere dysfunction due to telomere attrition. However, the diversity in senescence parameters among cells from different tissues, organs, and species, exposed to different types of stresses, suggests caution in extrapolating results among cell types. We were surprised that activated p53 was not detected in either 184 or 48 HMFC at senescence, although it has been seen in other senescent human fibroblasts (35). This result could be related to prior studies showing elevated levels of p16, but not p21, in these HMFC populations at senescence (5). Both cultured HMEC and HMFC may be similar in their preferential use of p16 and not p21 to enforce stasis. We have speculated that induction of p21 may result from p53-inducing stresses such as endogenous oxidative damage; mammary gland-derived cells may be less vulnerable to oxidative damage than e.g., keratinocytes or fetal fibroblasts.

Oxidative damage may occur preferentially at telomeres due to their high guanine triplet content and less efficient DNA damage repair (46), which can lead to a DNA damage response exhibiting foci at telomeres. Telomere erosion is also accelerated in some cell types exposed to hyperoxia; severe hyperoxia-induced telomere attrition in human fetal fibroblasts led to detectable genomic instability prior to a full DNA damage-induced arrest (47). Nonetheless, most reports do not demonstrate critically short telomeres or genomic instability in senescent human fibroblasts (48), and their senescence arrest could be, in part, a consequence of an elicited DNA damage response showing preferential damage at the telomeric ends, rather than from telomere attrition per se. This distinction is significant because, at least in HMEC, telomere dysfunction from telomere attrition is associated with widespread genomic instability, whereas cells at stasis have normal genomes. Telomerase reactivation is required to overcome the proliferation barrier resulting from telomere attrition, but is not necessary or sufficient to overcome a telomere-length independent p53-dependent DNA damage response. This distinction may also be significant for modeling malignant progression; genomic instability and telomerase reactivation are first seen at the DCIS stage, and are not found in atypical hyperplasia (5,9,15,16). We have proposed that the genomic instability seen in HMEC with telomere dysfunction due to telomere attrition may give rise to errors allowing telomerase reactivation (49).

In summary, we have developed culture conditions that allow long-term growth of HMEC with markers found in both myoepithelial and luminal epithelial HMEC lineages in vivo. This increased proliferative potential facilitates studies on the molecular properties of growing and senescent normal HMEC, as well as their use for high throughput examination of pro- and anti-aging or carcinogenic factors. The senescence barrier encountered by these cells, stasis, is not associated with critically short telomeres or genomic instability, in contrast to the telomere dysfunction barrier, agonescence, encountered by the p16(−), p53(+) post-selection HMEC that have overcome stasis. Isogenic HMFC at senescence arrest express properties more similar to HMEC at stasis than agonescence. Our data suggest that the senescence barrier encountered by genomically unperturbed human epithelial and fibroblast cells in culture may be primarily a consequence of exposure to stresses rather than telomere attrition.

Supplementary Material

Refer to Web version on PubMed Central for supplementary material.

Acknowledgments

This work was supported by NIH CA112970 (JCG, SB, BM, HF, AJW, MRS), NIH CA24844 (JCG, MRS), the Director, Office of Science, Office of Biological & Environmental Research, of the U.S. Department of Energy under Contract No. DE-AC02-05CH11231 (JCG, SB, BM, HF, AJW, MRS), and Ruth L. Kirschstein National Research Service Award Individual Fellowship CA108480-03 (EB). We thank the Colorado Genetics Laboratory, University

of Colorado Health Sciences Center for support in G-banding and imaging metaphase chromosomes, and Shalini Varghese and Stefan Vanderweil for technical assistance.

Abbreviations

A	lipid-rich bovine serum albumin
CT	cholera toxin
CKI	cyclin dependent kinase inhibitor
CM	conditioned media
HMEC	human mammary epithelial cells
HMFC	human mammary fibroblast cells
IF	immunofluorescence
IHC	immunohistochemistry
K	keratin
LI	labeling index
p	passage
PCA	Principal Component Analysis
PD	population doublings
PT	partial trypsinization
Rb	retinoblastoma protein
SA-β-Gal	senescence associated β-galactosidase
TRF	terminal restriction fragment
X	oxytocin

References

1. Stampfer MR. Cholera toxin stimulation of human mammary epithelial cells in culture. In Vitro 1982;18:531–7. [PubMed: 6288550]
2. Hammond SL, Ham RG, Stampfer MR. Serum-free growth of human mammary epithelial cells: Rapid clonal growth in defined medium and extended serial passage with pituitary extract. Proc Natl Acad Sci U S A 1984;81:5435–9. [PubMed: 6591199]
3. Ramirez RD, Morales CP, Herbert BS, et al. Putative telomere-independent mechanisms of replicative aging reflect inadequate growth conditions. Genes Dev 2001;15:398–03. [PubMed: 11230148]
4. Rheinwald JG, Hahn WC, Ramsey MR, et al. A two-stage, $p16^{INK4a}$-and p53-dependent keratinocyte senescence mechanism that limits replicative potential independent of telomere status. Mol Cell Biol 2002;22:5157–72. [PubMed: 12077343]
5. Romanov S, Kozakiewicz K, Holst C, Stampfer MR, Haupt LM, Tlsty T. Normal human mammary epithelial cells spontaneously escape senescence and acquire genomic changes. Nature 2001;409:633–7. [PubMed: 11214324]
6. Stampfer MR, Bartley JC. Induction of transformation and continuous cell lines from normal human mammary epithelial cells after exposure to benzo(a)pyrene. Proc Natl Acad Sci U S A 1985;82:2394–8. [PubMed: 3857588]

7. Stampfer MR, Bartley JC. Human mammary epithelial cells in culture: differentiation and transformation. Cancer Treat Res 1988;40:1–24. [PubMed: 2908646]
8. Brenner AJ, Stampfer MR, Aldaz CM. Increased p16INK4a expression with onset of senescence of human mammary epithelial cells and extended growth capacity with inactivation. Oncogene 1998;17:199–05. [PubMed: 9674704]
9. Garbe JC, Holst CR, Bassett E, Tlsty T, Stampfer MR. Inactivation of p53 function in cultured human mammary epithelial cells turns the telomere-length dependent senescence barrier from agonescence into crisis. Cell Cycle 2007;6:1927–36. [PubMed: 17671422]
10. Crawford YG, Gauthier ML, Joubel A, et al. Histologically normal human mammary epithelia with silenced p16(INK4a) overexpress COX-2, promoting a premalignant program. Cancer Cell 2004;5:263–73. [PubMed: 15050918]
11. McDermott KM, Zhang J, Holst CR, Kozakiewicz BK, Singla V, Tlsty TD. p16(INK4a) prevents centrosome dysfunction and genomic instability in primary cells. PLoS Biol 2006;4:e51. [PubMed: 16464125]
12. Zhang J, Pickering CR, Holst CR, Gauthier ML, Tlsty TD. p16INK4a modulates p53 in primary human mammary epithelial cells. Cancer Res 2006;66:10325–31. [PubMed: 17079452]
13. Li Y, Pan J, Li JL, et al. Transcriptional changes associated with breast cancer occur as normal human mammary epithelial cells overcome senescence barriers and become immortalized. Mol Cancer 2007;6:7. [PubMed: 17233903]
14. Novak P, Jensen TJ, Garbe JC, Stampfer MR, Futscher BW. Step-wise DNA methylation changes are linked to escape from defined proliferation barriers and mammary epithelial cell immortalization. Cancer Res 2009;67:5251–8. [PubMed: 19509227]
15. Stampfer MR, Bodnar A, Garbe J, et al. Gradual phenotypic conversion associated with immortalization of cultured human mammary epithelial cells. Mol Biol Cell 1997;8:2391–05. [PubMed: 9398663]
16. Chin K, Ortiz de Solorzano C, Knowles D, et al. In situ analysis of genome instability in breast cancer. Nature Genetics 2004;36:984–8. [PubMed: 15300252]
17. Tlsty TD, Romanov SR, Kozakiewicz BK, Holst CR, Haupt LM, Crawford YG. Loss of chromosomal integrity in human mammary epithelial cells subsequent to escape from senescence. J Mammary Gland Biol Neoplasia 2001;6:235–43. [PubMed: 11501583]
18. Stampfer MR. Isolation and growth of human mammary epithelial cells. J Tissue Culture Methods 1985;9:107–16.
19. Stampfer, M.; Yaswen, P. Culture systems for study of human mammary epithelial cell proliferation, differentiation and transformation. In: Taylor-Papadimitriou, J., editor. Cancer Surveys Vol. 18: Breast Cancer. New York: Cold Spring Harbor; 1994. p. 7-34.
20. Stampfer M, Garbe J, Levine G, Lichsteiner S, Vasserot A, Yaswen P. Expression of the telomerase catalytic subunit, hTERT, induces resistance to transforming growth factor β growth inhibition in $p16^{INK4}$ (−) human mammary epithelial cells. Proc Natl Acad Sci U S A 2001;98:4498–03. [PubMed: 11287649]
21. Dimri GP, Lee X, Basile G, et al. A novel biomarker identifies senescent human cells in culture and in aging skin in vivo. Proc Natl Acad Sci U S A 1995;92:9363–7. [PubMed: 7568133]
22. Allsopp RC, Vaziri H, Patterson C, et al. Telomere length predicts replicative capacity of human fibroblasts. Proc Natl Acad Sci U S A 1992;89:10114–8. [PubMed: 1438199]
23. Gustashaw, KM. Chromosome Stains. In: Barch, MJ.; Knutsen, T.; Spurbeck, JL., editors. The AGT Cytogenetics Laboratory Manual. Vol. 3. Philadelphia: Lippincott-Raven; 1997. p. 269-80.
24. Smyth, GK. Limma: linear models for microarray data. In: Gentleman, R.; Carey, V.; Dudoit, S.; Irizarry, R.; Huber, W., editors. Bioinformatics and Computational Biology Solutions using R and Bioconductor. New York: Springer; 2005. p. 397-20.
25. Smyth GK. Linear models and empirical bayes methods for assessing differential expression in microarray experiments. Stat Appl Genet Mol Biol 2004;3Article3
26. Benjamini Y, Hochberg Y. Controlling the false discovery rate: a practical and powerful approach to multiple testing. J R Statist Soc B 1995;57:289–00.
27. Eisen MB, Spellman PT, Brown PO, Botstein D. Cluster analysis and display of genome-wide expression patterns. Proc Natl Acad Sci U S A 1998;95:14863–8. [PubMed: 9843981]

28. Jolliffe, IT. Principal Component Analysis. Vol. XXIX. New York: Springer; 2002.
29. Dennis G Jr, Sherman BT, Hosack DA, et al. DAVID: Database for Annotation, Visualization, and Integrated Discovery. Genome Biol 2003;4:P3. [PubMed: 12734009]
30. Stampfer MR, Hallowes R, Hackett AJ. Growth of normal human mammary epithelial cells in culture. In Vitro 1980;16:415–25. [PubMed: 6993343]
31. Garbe J, Wong M, Wigington D, Yaswen P, Stampfer MR. Viral oncogenes accelerate conversion to immortality of cultured human mammary epithelial cells. Oncogene 1999;18:2169–80. [PubMed: 10327063]
32. Taylor-Papadimitriou J, Stampfer MR, Bartek J, Lane EB, Lewis A. Keratin expression in human mammary epithelial cells cultured from normal and malignant tissue: Relation to in vivo phenotypes and influence of medium. J Cell Sci 1989;94:403–13. [PubMed: 2483723]
33. Villadsen R, Fridriksdottir AJ, Ronnov-Jessen L, et al. Evidence for a stem cell hierarchy in the adult human breast. J Cell Biol 2007;177:87–01. [PubMed: 17420292]
34. Sedelnikova OA, Horikawa I, Zimonjic DB, Popescu NC, Bonner WM, Barrett JC. Senescing human cells and ageing mice accumulate DNA lesions with unrepairable double-strand breaks. Nat Cell Biol 2004;6:168–70. [PubMed: 14755273]
35. Campisi J, d'Adda di Fagagna F. Cellular senescence: when bad things happen to good cells. Nat Rev Mol Cell Biol 2007;8:729–40. [PubMed: 17667954]
36. Olsen CL, Gardie B, Yaswen P, Stampfer MR. Raf-1-induced growth arrest in human mammary epithelial cells is p16-independent and is overcome in immortal cells during conversion. Oncogene 2002;21:6328–39. [PubMed: 12214273]
37. Ince TA, Richardson AL, Bell GW, et al. Transformation of different human breast epithelial cell types leads to distinct tumor phenotypes. Cancer Cell 2007;12:160–70. [PubMed: 17692807]
38. Uvnas Moberg, K. The Oxytocin Factor. Cambridge: Da Capo Press; 2003.
39. Bocker D, Verspohl EJ. Role of protein kinase C, PI3-kinase and tyrosine kinase in activation of MAP kinase by glucose and agonists of G-protein coupled receptors in INS-1 cells. Int J Exp Diabetes Res 2001;2:233–44. [PubMed: 12369712]
40. Cassoni P, Marrocco T, Deaglio S, Sapino A, Bussolati G. Biological relevance of oxytocin and oxytocin receptors in cancer cells and primary tumors. Ann Oncol 2001;12 (Suppl 2):S37–39. [PubMed: 11762350]
41. Bussolati G, Cassoni P. Editorial: the oxytocin/oxytocin receptor system-expect the unexpected. Endocrinology 2001;142:1377–9. [PubMed: 11250915]
42. Rimoldi V, Reversi A, Taverna E, et al. Oxytocin receptor elicits different EGFR/MAPK activation patterns depending on its localization in caveolin-1 enriched domains. Oncogene 2003;22:6054–60. [PubMed: 12955084]
43. Sapino A, Macri L, Tonda L, Bussolati G. Oxytocin enhances myoepithelial cell differentiation and proliferation in the mouse mammary gland. Endocrinology 1993;133:838–42. [PubMed: 8344220]
44. Bartley JC, Stampfer MR. Factors influencing benzo(a)pyrene metabolism in human mammary epithelial cells in culture. Carcinogenesis 1985;6:1017–22. [PubMed: 4017169]
45. Zhang H, Pan KH, Cohen SN. Senescence-specific gene expression fingerprints reveal cell-type-dependent physical clustering of up-regulated chromosomal loci. Proc Natl Acad Sci U S A 2003;100:3251–6. [PubMed: 12626749]
46. Passos JF, Saretzki G, von Zglinicki T. DNA damage in telomeres and mitochondria during cellular senescence: is there a connection? Nucleic Acids Res 2007;35:7505–13. [PubMed: 17986462]
47. Ahmed S, Passos JF, Birket MJ, et al. Telomerase does not counteract telomere shortening but protects mitochondrial function under oxidative stress. J Cell Sci 2008;121:1046–53. [PubMed: 18334557]
48. Li GZ, Eller MS, Firoozabadi R, Gilchrest BA. Evidence that exposure of the telomere 3′ overhang sequence induces senescence. Proc Natl Acad Sci U S A 2003;100:527–31. [PubMed: 12515865]
49. Stampfer MR, Yaswen P. Human epithelial cell immortalization as a step in carcinogenesis. Cancer Lett 2003;194:199–08. [PubMed: 12757978]
50. Stampfer MR, Garbe J, Nijjar T, Wigington D, Swisshelm K, Yaswen P. Loss of p53 function accelerates acquisition of telomerase activity in indefinite lifespan human mammary epithelial cell lines. Oncogene 2003;22:5238–51. [PubMed: 12917625]

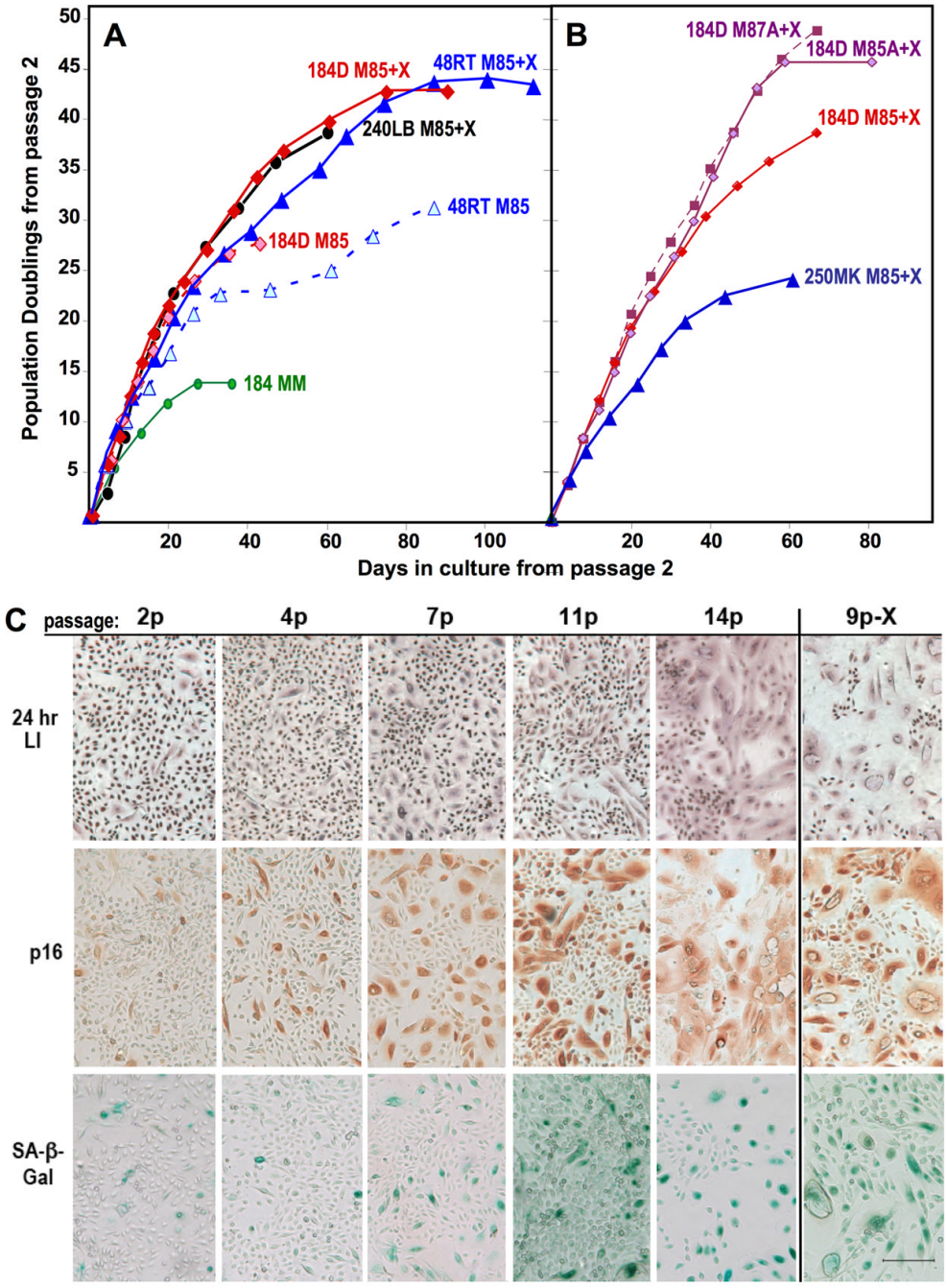

Figure 1.

Growth of pre-stasis HMEC in M85 or M87 ± oxytocin (X) or BSA (A). A. Primary cultures from three reduction mammoplasty specimens were started from organoids and grown in M85 ±X. The number of PD in primary culture cannot be accurately determined; growth is shown starting from 2p with cells obtained from PT 2. Each point represents cell counts at successive passage levels, e.g., the final points shown in 1A for 184D 48RT, and 240LB grown in M85 +X are respectively 16p, 17p, and 11p. All media contained cholera toxin from passage 2. B. Frozen stocks of second pasasge184D HMEC from PT 3 were grown in media with (M85) or without (M87) CM ± lipid rich BSA (A), in the presence of oxytocin. 250MK are derived from milk, grown in MM for primary culture, then switched to M85+X at second passage. C.

Expression of markers associated with proliferation (LI) and senescence (p16, SA-β-Gal) in pre-stasis 184 HMEC with increasing passage. All cells except for 9p-X were grown in M85 with oxytocin; stasis in this population was at 15p. The 9p-X culture was grown in M85 without oxytocin; stasis was at 10p. Cultures examined are from the growth curve shown in Fig. 1A. Note the reciprocal relationship between the small cells with a positive LI, and the larger, often vacuolated cells that are positive for p16 and SA-β-Gal, and negative for LI. Size marker = 200 microns.

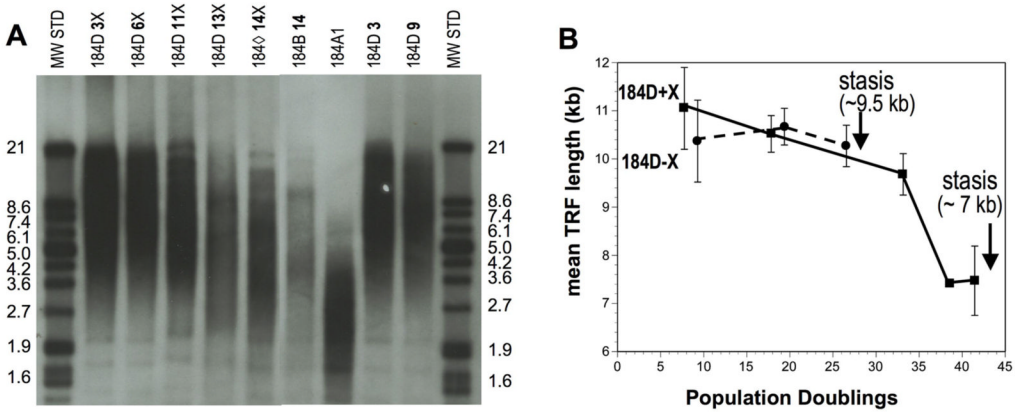

Figure 2.

Mean TRF length of pre-stasis 184D HMEC with increasing passage. Pre-stasis HMEC are from Fig. 1A. Agonescent post-selection HMEC (184B 14p), and the immortally transformed line 184A1, are shown for comparison; 184A1 has a reported mean TRF length of ~3–5 kb, agonescent 184 HMEC have a reported faint signal with a mean TRF of ≤ 5 kb (15,50). Molecular weight standards are shown on the outside lanes. A. Representative gel; B. Calculated mean TRF values from 3 independent gels (1 sample only at 13p).

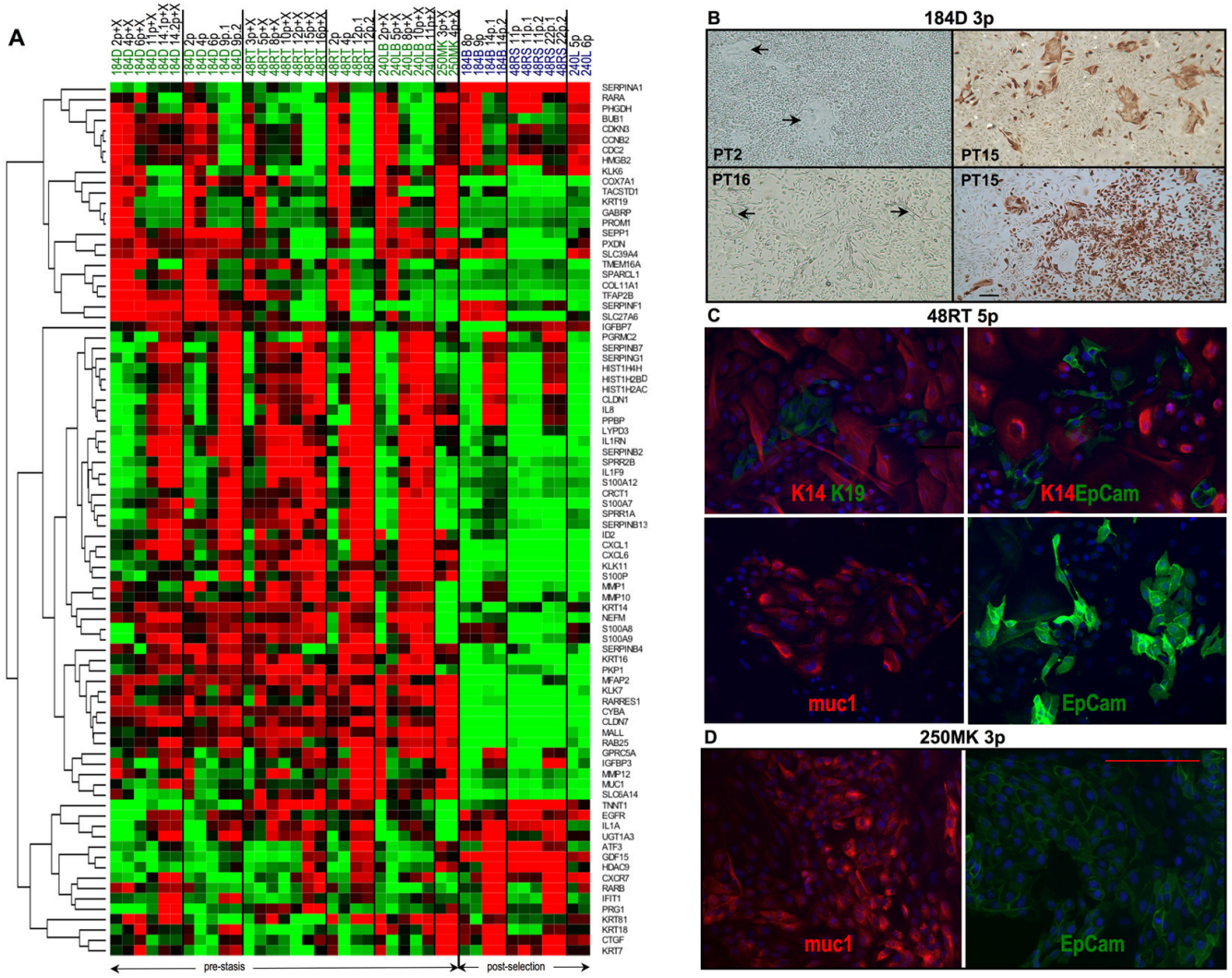

Figure 3.

Gene transcript and protein expression in pre-stasis HMEC from different individuals. A. Hierarchical clustering (by rows) of gene transcript profiles in growing and senescent pre-stasis and post-selection HMEC. Pre-stasis 184D, 48RT, and 240LB HMEC (from figure 1A) are shown in columns with increasing passage (p) up to stasis; (X) indicates growth in oxytocin. Post-selection 184B and 48RS HMEC are growing and agonescent populations. Genes shown are 77 selected for the greatest variance across all samples, plus a few selected lineage or differentiation-associated genes. B. Morphology and K19 expression in pre-stasis 184D HMEC grown in M85+X at passage 3: A culture from PT 2 shows cobblestone and closed colony (arrows) morphologies, while a culture from PT 16 shows more heterogeneous morphologies, including cells with cytoplasm that extends over other cells (arrows). Cultures from PT 15 stained for K19 by IHC show the presence of K19 protein in cells with the closed colony morphology as well as in some areas with cobblestone and extended morphologies. Size marker = 200 microns. C. Lineage markers in 48RT passage 5 (from PT 5) stained by IF. Cultures show cells displaying luminal markers (K19, EpCam, muc1) interspersed with cells displaying myoepithelial lineage marker (K14) and as small homogeneous patches. D. Lineage markers in 250MK passage 3 illustrate a luminal phenotype. Size marker = 200 microns.

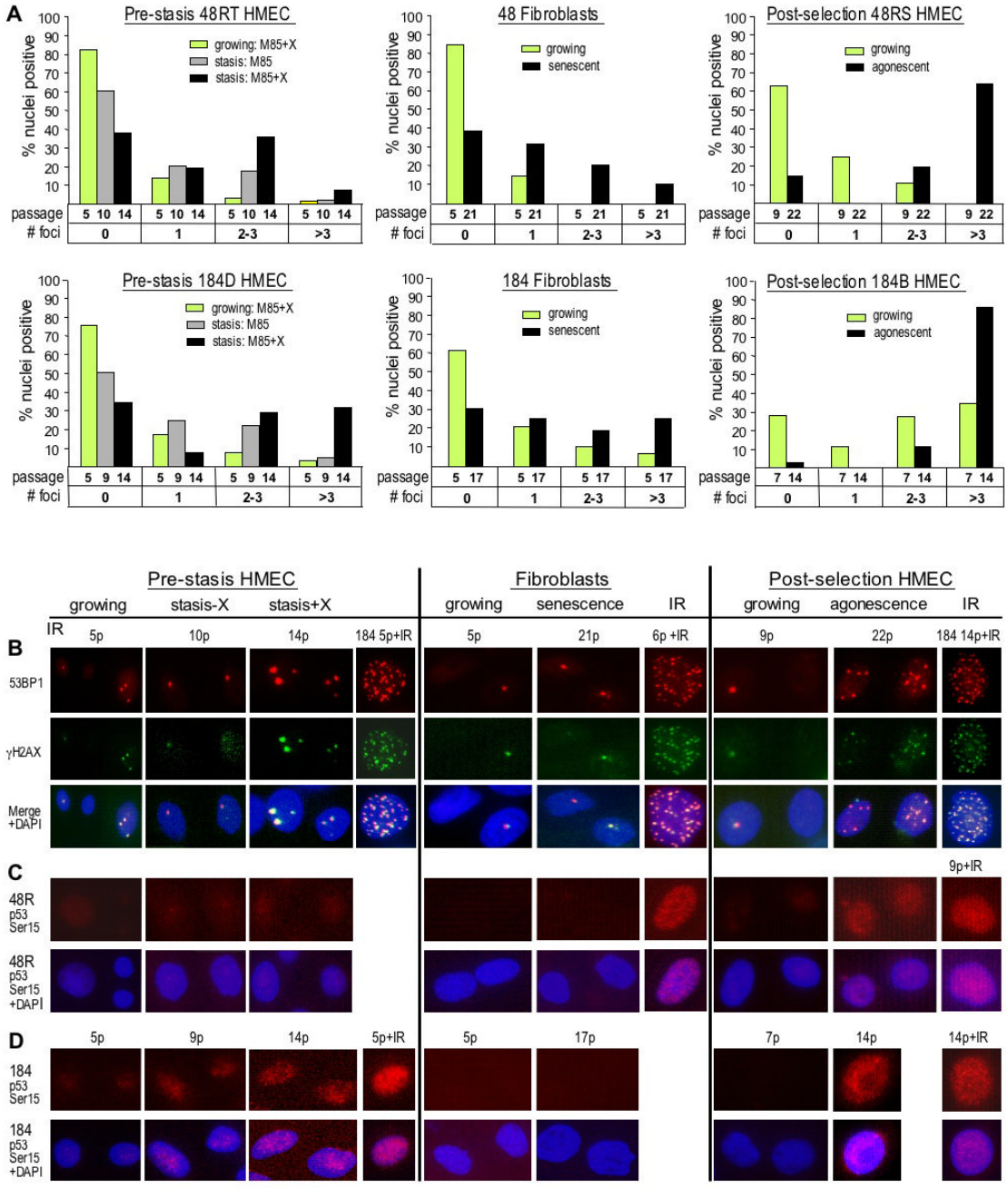

Figure 4.

Markers of DNA damage in growing and senescent pre-stasis and post-selection HMEC, and isogenic HMFC. Senescent cultures were examined one passage prior to when cultures showed no net increase in cell number. A. 53BP1 foci; Note the higher level of foci in agonescent HMEC compared to senescent HMFC or HMEC at stasis, and the higher level of foci in cells from specimen 184 compared to specimen 48. B–D. Representative IF images of growing and senescent pre-stasis and post-selection HMEC, and isogenic HMFC. B: 53BP1 and γH2AX foci in specimen 48; C–D: activated p53 in specimens 48 and 184. Cells exposed to 10 Gy of IR are shown as positive controls. Note the greater number of foci, and higher level of serine15-

phosphorylated p53 in agonescent HMEC compared to senescent HMFC or HMEC at stasis. Cultures examined are from the growth curve shown in Fig. 1A.

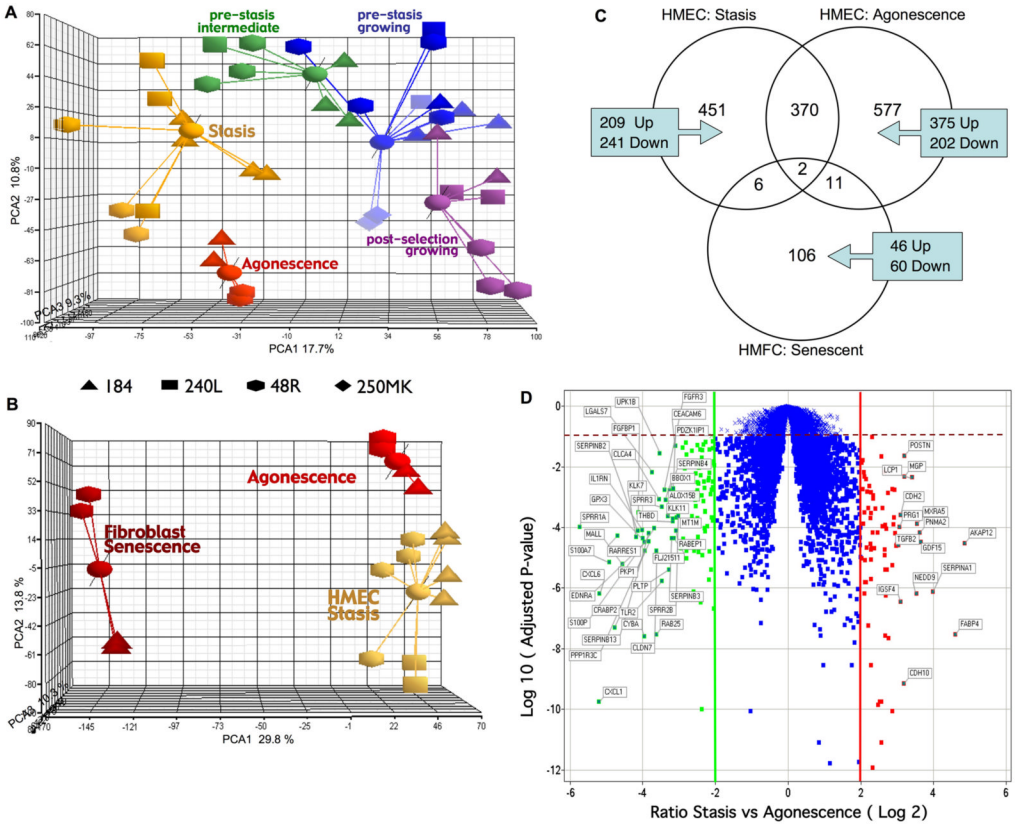

Figure 5.

Relationship of growing and senescent HMEC and HMFC as determined by transcriptional profiles. A. PCA plot of transcriptional profiles of growing and senescent pre-stasis and post-selection HMEC. B. PCA plot of transcriptional profiles of all senescent HMEC and HMFC. The 3D scatter plots show the first three principal components of the analysis of 9702 genes. Data points from different individuals are represented by different shapes. C. Venn diagram of genes modulated at HMEC stasis using growing pre stasis as baseline, at HMEC agonescence using growing post selection as baseline, or at HMFC senescence with growing fibroblast as baseline. Diagram depicts the number of genes unique to each group and the number that overlap between and among the groups. D. Volcano plot illustrating genes significantly differentially expressed between stasis vs. agonescence. The x- axis represents the fold change ratio (log2) between HMEC at stasis and agonescence. The y-axis represents the significance with adjusted *p*-values. The graph is segmented to represent the genes that satisfy the fold change criteria of +/− 2 and adjusted $p < 0.1$. Segments on right and left show the genes up-regulated at agonescence (79) and stasis (116) respectively. Genes with more then eight fold change difference between stasis and agonescence are labeled.

Table 1

FACS analysis of growing and senescent HMEC

Cell ID	Medium	Passage	Status	G0/G1	S	G2/M
184D	M85+X	4	growing	60.9*	20.2	18.9
184D	M85+X	15	stasis	89.4	0.	10.6
184D	M85	10	stasis	81.8	9.7	8.4
184B	MCDB170	10	growing	62.4	19.2	18.4
48RT	M85+X	14	stasis	87	0.4	12.6
48RT	M85	10	stasis	88	3.0	9.0

* percentage of cells in the different cell cycle phases